Improving the experimental protocol for a more accurate identification of a given mechanical behavior in a single assay: application to skin

Jean-Sébastien Affagard, Florent Wijanto, Jean-Marc Allain

Improving the experimental protocol for a more accurate identification of a given mechanical behavior in a single assay: application to skin

J-S. AFFAGARD , F. WIJANTO , J-M. ALLAIN*

LMS, École polytechnique, CNRS, Université Paris-Saclay, Palaiseau, France

Inria, Université Paris-Saclay, Palaiseau, France

* {allain@lms.polytechnique.fr}

Abstract

Mechanical properties of the skin, the external organ of the human body, are important for many applications such as surgery or cosmetics. Due to the highly hierarchical structure of the tissue, it is interesting to develop microstructural models which have a better predictability and should reduce the consequences of the sample variability. However, these models generally include a quite large number of mechanical parameters. Therefore, complex assays are required to achieve a proper identification of the microstructural models. We investigated here the best experimental protocol to identify a non-linear, anisotropic, model of skin behavior, namely the Holzapfel's law, using displacement field and force measurements. This was done through a sensitivity analysis of the different parameters. We determined first the

optimal assay, which appears to be a biaxial test with an alternated loading: first a stretch in one direction, then in the perpendicular one, and so on. To further improve the quality of the assay, we also determined the optimal geometry. Interestingly, slightly asymmetric geometries are more adequate than symmetric ones, while being easier to realize.

Keywords: *biomechanics, biaxial traction, large strain, anisotropy, sensitivity*

1 Introduction

Skin is the outer cover of birds, reptiles and mammalian bodies, with an important protective role as the first barrier against external pathogens. As the skin is also protecting against shocks or loss of water, it plays a key role in the comfort for daily life. Our appraisal of age and beauty are also strongly related to the skin external aspect. Thus, a good understanding of the mechanical behavior of skin is useful for many applications, ranging from the cosmetic industry to the design of devices such as wheelchairs or razors, for which the stress distribution is likely to be an ergonomic indicator. For the simpler cases, a macroscopic description will be sufficient. However, a finer description of the skin is often useful, to predict fine geometrical effects [1], but also to predict the consequence of an alteration of the microstructure due to either ageing [2, 3, 4], pathologies [5, 6] or surgeries [7].

Skin is made of 3 distinct layers: the epidermis, the dermis and the hypodermis, from the outside to the inside. The epidermis is a superficial layer composed of living cells and cellular debris. The dermis is a connective

tissue, composed of fibers (mostly collagen with elastin) embedded in a soft disorganized matrix of water and biomolecules, with very few cells inside. Collagen fibers represent $70 - 80\%$ of the dry weight [8], and have a strong hierarchical organization, ranging from a few to hundred of nanometers; it is well admitted that their spatial organization impacts strongly the mechanical properties of the skin [9]. The hypodermis consists mostly of fat, in a loose connective tissue.

Skin macroscopic mechanical behavior is highly anisotropic, heterogeneous with a non-linear viscoelastic and quasi-incompressible behavior [10, 11]. The typical nominal stress *vs.* stretch response has the so-called "J-shape" and is usually described with 3 parts [12]: the initial "toe" region where the stretch doesn't generate significant forces, then the "heel" region where the force increases non-linearly with the stretch and finally the "linear" part where the force increases linearly with the stretch. After these regions, an irreversible breaking occurs. The classical microstructural interpretation of this behavior assumes that most of the stress comes from the collagen fibers. Initially, they are crimped, and they unfold in the "toe" region, so the stress is mostly due to the matrix and the elastin. In the "heel" region, the fibers align themselves into the direction of traction, and finally, the linear part is due to the elastic responses of the aligned fibers. However, this interpretation has been recently challenged by experimental observations [5, 13].

As the outer organ, the skin is easy to access *in vivo*: mechanical tests directly on the human or the animal are in a more physiological state than *ex vivo* ones. A large range of tests have been used for *in vivo* characteriza-

tion: static ones such as suction [14, 15, 16, 17], indentation [18, 19, 20, 21] and torsion [22, 23], and dynamic ones such as MRE (Magnetic Resonance Elastography) [24] or ultrasound elastography [25, 26]. It is even possible to measure the anisotropic response, for example by coupling an optical method with mechanical test [27, 28, 29, 30]. Due to the complex structure of the skin, a final identification procedure (classically based on Finite Element Model Updating - FEMU) has to be performed to determine the mechanical parameters, assuming a behavior law as Ogden [31], Fung [32] or Holzapfel [33] for each layer.

The intrinsic limitations of the *in vivo* assays made them unsuitable to analyze carefully the relationship between microstructure and mechanical properties: on top of requiring an animal, they are limited to a small range of stretch and stress distribution is obtained through the assumed behavior law. Therefore, *ex vivo* experiments are much more frequent, with two main types: uniaxial traction and multiaxial sollicitations. Monotonic tension tests give easily access to the primary biomechanical performances such as elastic modulus and ultimate tensile strength [12, 34, 35, 10]. To go further in the skin mechanical behavior description, the viscoelastic properties were characterized through various strain rates [36, 37, 38], relaxation or creep test [39]. Finally, the preconditioning and fatigue were assessed thanks to uniaxial cyclic loading [40].

Multiaxial sollicitations are more complex to perform but are more relevant to characterize the influence of the microstructure [41, 42]. Indeed, in Refs. [43, 44], a biaxial traction assay was compared with a uniaxial traction. The results highlighted the relaxation differences induced by the

transverse loading, and a structural theory of flat collageneous tissues was then proposed [45]. In Ref. [46], a multi-axial experiment was designed to characterize the two dimensional elastic properties of human skin. In Ref. [35, 47] the deformation field was measured on skin tissue by drawing a fine grid: strong non-linearities originating from the reorganization of the collagen fibers were then reported. Finally, in ref. [48] a multiaxial test was performed and then a cross correlation technique allowed measuring a displacement field, used to identify a Holzapfel-like behavior [33].

Biaxial tests are the most frequent type of multiaxial assays. The difficulties associated with the geometry and the structure of the specimens have been well highlighted in the literature. For example, the measures are sensitive to the fine positioning (spacing and alignment) of suture attachment points [49], which may induce stress concentrations in the specimen [50]. In Ref [51, 52], finite element simulations of a biaxial clamp experiment were performed to quantify the stress-shielding, and to create a correction factor. An illustration of the dependence on sample geometry and material anisotropy was shown in the same paper. These problematics are found in all biaxial tests, even in linear materials such as steel. In Ref. [53], a FEMU approach was developed on sheet steel metal to numerically compare the identification accuracy between several biaxial tests. In Ref. [54], an original approach based on the sensitivity analysis was proposed to design and to optimize the shape of a biaxial clamp test to identify the elastoplastic properties of stainless steel.

In this present study, we proposed a methodology to optimize the identification of the mechanical parameter for skin. It is important to keep in mind

that specific constraints apply to biological samples, the most important one being the variability between two samples. Thus, our aim is to extract as much information as possible form a single assay, which has to be realistic and in particular, doable in a reasonable time. The general approach consists in performing a sensitivity analysis to illustrate the identification accuracy (*i.e.* the influence of a parameter variation on each measured quantity) on each parameter. This is complex for the general case. Therefore, we have chosen to work on a frequently-used test that will be improved to determine the parameters of an already known constitutive equation. Here, we have used the classical Holzapfel's law. Our approach could have been applied to other constitutive equations without difficulties, and the conclusions would have likely been the same. The known quantities here are the grips forces and displacements, as well as the full field of displacement. Such types of identification approaches are frequently used in the literature (for a review, see [55]). We have chosen here to determine the best loading path among three realistic ones: uniaxial, equibiaxial and alternated loading. Then, we have investigated the influence of the sample geometry on the sensitivity. Finally, a real geometry was analyzed, showing the benefits of asymmetrical imperfections for sensitivity analysis.

2 Materials and Methods

2.1 Experimental background

For the optimization, we based our approach on a protocol inspired from [5, 56], which is very similar to other uniaxial assays in biological membranes, and especially in skin. The only real specificity is that these experiments

were done on one-month old mice, shaved and with the epidermis removed. Just before experiment, each sample was cut and then covered with graphite powder (see fig.1a,b) to create the speckle pattern enabling the measurement of the displacement field with Digital Image Correlation (DIC). The sample was afterward fixed in the holding jaws of a symmetrical traction device (uniaxial or biaxial). Each motor (two or four) supports a load cell on which a jaw was screwed (see fig.1c).

Traction was performed at constant motor velocities (imposing the displacement of the grips). During the whole traction, the force on each arm is recorded and images of the sample were taken using a CCD camera. Constant hydration was preserved by spraying mineral water on the sample every three minutes. This could alter the speckle pattern during the assay in few points; these points have to be subsequently removed from the analysis. The displacement field was then measured using CMV software (CorrelManuV [57]), which does a local correlation of the gray levels between subimages.

2.2 Numerical model

The sensibility analyses were performed on FEM (Finite Element Method) simulations, with different geometries and for different loading paths.

2.2.1 Constitutive behavior

Skin is classically considered as an incompressible, anisotropic, hyperelastic material, with a "J-shape" stress-stretch curve [5]. A frequently-used Holzapfel's behavior was chosen to describe the mechanical response of the skin [33, 58]:

$$W = C_{10}(\overline{I}_1 - 3) + \frac{k_1}{2k_2}\left(e^{k_2<\overline{E}_\alpha>^2} - 1\right) \quad (1)$$

where C_{10} describe the non-collagenous isotropic ground material behavior and k_1 and k_2 the contributions from the different families of collagen fibers. $\overline{I}_1$ is the first deviatoric strain invariant defined as: $\overline{I}_1 = J^{-2/3} I_1$, with $J = det(\underline{\underline{F}})$, and $I = tr(\underline{\underline{F}}^T \underline{\underline{F}})$, $\underline{\underline{F}}$ being the deformation gradient tensor. $\overline{E}_\alpha$ is a strain-like quantity that characterizes the deformation of fibers in their mean direction:

$$\overline{E}_\alpha = \kappa(\overline{I}_1 - 3) + (1 - 3\kappa)(\overline{I}_{4(\alpha\alpha)} - 1) \tag{2}$$

where the κ parameter describes the level of fiber dispersion along the mean direction with $(0 \leq \kappa \leq 1/3)$. When $\kappa = 0$, the fibers are perfectly aligned, and when $\kappa = 1/3$ the fibers are randomly distributed and the material is isotropic. The pseudo-invariant $\overline{I}_{4(\alpha\alpha)}$ represents the square of the stretch ratio in the fiber direction α. The operator $< . >$ is defined as $< x >= \frac{1}{2}(|x| + x)$ (i.e.: $< \overline{E}_\alpha > \geq 0$) so that the fibers are contributing to the stress only when in traction. We have considered a single family of fibers, based on experimental observations of the microstructure [5]. These fibers are the main source of anisotropy in the tissue. For other tissues, it may be more relevant to use more orientations or more families.

This model assumes that the skin is incompressible. Such an assumption is considered to describe correctly the behavior of the skin [10]. The model also doesn't describe viscous behavior, damage or breaking of the tissue. This could be done, but the model will then request more parameters and therefore more complex loadings to be fully determined. In particular, measurement of cycles of stretching or of relaxations at different levels in a single experiment will lengthen the experiment significantly. Thus, we have

used a classical hyperelastic law. As the viscosity in not predominant for low strain rate, this seems an adequate simplification.

The samples were considered to have homogeneous mechanical properties: the parameters of the energy did not depend on the location as shown in previous experiments [5]. It could have been possible to consider heterogeneous materials, albeit with the difficulty that the identification will be possible only in the regions were the model is sensitive enough. Similarly, we could have used more complex constitutive behaviors (with dissipation, viscosity or damage). These behaviors are less frequently used for biological membranes; Due to their complexity, the protocol is heavier to improve, even if it could be done through an approach similar to ours. However, they are more complex to identify in a single experiment.

2.2.2 Mesh generation

The computational model was ran on Abaqus software ([59]). Two different types of mesh were generated: realistic ones to be compared with the experimental data, and idealized ones to test the sensibility to the geometry. In all cases, the plane stress assumption was considered, the thickness being very small with respect to the other sizes.

Realistic meshes were created so that the experimental measures of the displacement can be directly compared to the results of the FE model. First, the geometry of the sample was obtained from the experimental sample image taken just before the traction. This image was also used as the reference image for the DIC, and the positions of the correlation points were extracted using a custom-written Matlab script (see fig.2a). The same script was then

used to segment the geometry of the sample, including a subset of all the correlation points (see fig.2b), and refined. The refinement was done so that an increase of the number of nodes induced a change smaller than the noise in the calculated forces and in the simulated displacements. However, too many nodes slow down the simulation, so the number of nodes was kept to a minimum. Thereby, 3-node linear (CPS3) meshes were created (see fig.2b).

The idealized meshes were created for both uniaxial and biaxial experiments, with respectively a dog-bone and a cross shape. Examples of idealized meshes are shown, with the adjustable geometrical parameters, respectively on figure 3a and 3b. The shape being symmetrical, only a quarter plate was meshed: Dirichlet conditions were imposed to fix the degrees of freedom in the symmetry directions (see fig.3a,b). For simplicity, we used 4-node linear (CPS4) meshes for the idealized geometries.

2.3 Determination of the loading pathway with a sensitivity analysis

As in the experimental protocol, the displacements of the grips were imposed in the simulation, assuming no slippage of the sample in the grips. For uniaxial loadings, the sample was stretched from 0 to 20% of macroscopic stretch. For biaxial loading, two loading paths were investigated (see fig.3c). First, a perfectly equibiaxial loading was considered, in which all the arms of the sample were stretched equivalently, up to 20% of macroscopic stretch. Second, an alternated loading was tested: the sample was initially stretched in the direction 1 by 10%, it was then stretched in the direction 2 by 20%, the stretch in 1 being maintained, and finally it was stretched up to 20%

in the direction 1 while the stretch in 2 was maintained (see fig.3c). These values were chosen based on our own experiments in order to be in the linear range (*i.e.* not in the heel region) during biaxial loading.

Figure 2c,d shows the simulated displacements U_1 and U_2, respectively in the horizontal and vertical directions, for an imposed stretch of 1.1 in direction 1 and of 1.2 in direction 2 on a realistic mesh. The mechanical parameters were in this case: $\alpha = 10°$, $C_{10} = 40kPa$, $k_1 = 0.8kPa$, $k_2 = 0.5kPa$ and $\kappa = 0.28$.

A sensibility analysis was performed on the idealized meshes to determine the optimal loading path for the identification of the 5 mechanical parameters. As in the experimental protocol, the displacements of the arms extremities were imposed. For the cross-shaped geometry, an equibiaxial test ($\epsilon_1 = \epsilon_2 = 0.2$) and an alternated test ($\epsilon_1 = 0.1, \epsilon_2 = 0$ and then $\epsilon_1 = 0.1, \epsilon_2 = 0.2$ and finally $\epsilon_1 = 0.2, \epsilon_2 = 0.2$) were simulated (see fig.3c). For the dog-bone geometry, an uniaxial stretching up to 20% was imposed in the direction of the sample. On each loading path, the displacement fields were extracted at each of the 8 steps (every 2.5% of stretching for the uniaxial and equibiaxial tests while it corresponds to 5% for the alternated test).

The sensitivity S_{P,θ_k} of a calculated quantity P (either a component of the displacement at a node, or a resultant force) quantifies the effect of a variation $\delta\theta_k$ of the parameter θ_k which is either a mechanical or geometrical parameter. S_{P,θ_k} is given by:

$$S_{P,t,\theta_k} = P(x, t, \theta_k + \delta\theta_k) - P(x, t, \theta_k). \tag{3}$$

The higher the sensitivity, the more influent the parameter on the quantity P and therefore the easier the identification of P will be. As the sensitivity depends on the current values of the parameters, the sensitivities were tested with respect to a reference set of parameters: $\alpha = 10°$, $C_{10} = 40kPa$, $k_1 = 0.8kPa$, $k_2 = 0.5$ and $\kappa = 0.28$. These parameters were chosen so that the predicted behavior would be similar to the experimental one [5], based on previous identifications of skin anisotropic hyperelastic behavior [48]. A variation of 1% was done for each mechanical parameter.

Finally, to illustrate the global sensitivity of each parameter, the sensitivity matrix M is constructed based on the vector of the sensitivities S_{θ_i}:

$$M_{ij} = \{S_{\theta_i}\}^T \{S_{\theta_j}\}. \tag{4}$$

The components of S_{θ_i} are the sensitivities of the quantities P to the parameter θ_i, for all the tested steps of the loading path. For example, the coefficient M_{11} is the sum of the square of the sensitivities of each displacement node and each force at each stretching step, for the parameter α of the behavior law.

3 Results

We intended to improve a classical biaxial experiment protocol for the identification of the five parameters of a complex hyperelastic behavior in a single experiment. To do so, we first investigated the consequences of different loading paths. Then, different geometries were studied. Finally, we illustrate the consequence of defects in perfectly symmetrical geometries

through the use of a real geometry.

3.1 Sensitivity analysis to determine the optimal loading path.

Figure 4 shows the displacement sensitivity maps for the uniaxial loading at the ultimate loading ($\epsilon_{xx} = 0.2$). Figure 5 shows the force sensitivity for the uniaxial loading at all steps. The displacements U_1 and U_2 and the force have a low sensitivity for the parameter k_2, related to the fiber stiffness. The displacement U_2 has a very localized sensitivity to most parameters, except the angle α for which the sensitivity is similar to the one of the U_1 field. This implies that a more complex loading, with more accessible data for U_2, is likely to provide more information. Therefore, biaxial loadings were tested.

Figure 6 shows the displacement sensitivity maps at ultimate loading of the equibiaxial loading experiment ($\epsilon_{xx} = \epsilon_{yy} = 0.2$); similarly, figure 7 shows the same maps at ultimate loading of the alternated loading experiment ($\epsilon_{xx} = 0.2$ and $\epsilon_{yy} = 0.1$). Figure 8 shows the two forces' sensitivity at all steps for equibiaxial (fig. 8a and b) and alternated loading (fig. 8c and d).

For the equibiaxial loading, as expected, each parameter has a maximal U_2 sensitivity close to the one in U_1, the differences being due to the anisotropy of the constitutive behavior. The sensitivity is maximal for the parameter κ, and is well spread on the whole surface of the sample. The parameters α, C_{10}, k_1 are also sensitive, although less so. However, the sensitivity of the parameter k_2 is very low, and an identification would be

difficult. The forces are sensitive mostly to the κ parameter, but also to the C_{10} and the k_1 parameters. However, the sensitivities to the parameters k_2 and the angle α are much lower (fig. 8a, b). Thus, the equibiaxial loading, although better than the uniaxial loading, remains insufficient to identify all the parameters with a high precision - and especially the parameter k_2. An important difficulty lies in the localization on the border of the sample of the maximum of sensitivity to some parameters (as C_{10} or k_2): it is the place where the displacement field measurement is the hardest to perform and likely the less accurate.

For the alternated loading, each parameter has a similar sensitivity in both directions, a non-obvious result. The values of the sensitivities are not very different from the ones for the equibiaxial loading. However, the maximum of the sensitivities are now inside the sample - the spatial distribution being different for each sensitivity. This is much more favorable for the identification of the parameters even if the contrast of sensitivity is not sufficient for the parameter k_2. Spatial distribution of U_1 and U_2 sensitivities for each parameter showed that the displacement determination should not focus on the center of the sample but more on the arms, and especially on the region just near the circular cuts. Sensitivities of the force to the different parameters are now of the same order of magnitude (see fig. 8c, d), apart for the parameter k_2.

Therefore, among our tested loading paths, the best one is the alternated loading. Still, it remains to be improved to increase the sensitivities (especially for the parameter k_2): this will be done by changing the sample geometry.

Figure 9 shows the sensitivity matrices for the alternated loading experiment. For the displacement fields (U_1 and U_2) and the force F_1, a strong maximal value is for the κ parameter, far above all the other ones. For the force F_2, the maximal value is for the C_{10} parameter, slightly above the other parameters, and two orders of magnitude below the sensitivities to the force in the direction 1.

The sensitivity matrix values reveal a similar influence in terms of global displacement sensibility for the two displacement fields. The U_1 sensitivity shows a high cross-sensitivity to three parameters: the angle α, k_1 and k_2, while the U_2 sensitivity matrix reveals a high cross-sensitivity to all parameters. Similarly, the forces F_1 and F_2 have a high cross-sensitivity to the three parameters C_{10}, k_1 and κ, while the influences of the angle and k_2 are low. Therefore, the influences of α, C_{10}, k_1 and k_2 will be difficult to separate during the identification process.

3.2 Influence of the geometry

3.2.1 Influence of the arm radius

Different radii were tested to obtain the best sensitivities in the alternated loading. Figure 10 shows the sensitivity maps of the parameter κ for the displacements U_1 and U_2, for three different mesh radii. An increase of the radius leads to a lower maximal sensitivity but spread on a larger region. Similar observations were obtained for all the parameters.

Consequently, the choice of radius doesn't appear to be critical for the identification of the material parameters. For practical reasons of sample manipulation and attachment, very small or large radii should be avoided.

The sensitivity analysis was done on an idealized geometry. In particular, the four arms are perfectly identical and symmetrical. Experimental realizations could not be as precise: the punches may not be perfectly positioned despite the use of a template, and the skin may deform differently during each punch. Therefore, we also tested the sensitivity for a real geometry.

3.2.2 Imperfect geometry: a real sample

Under real conditions of cutting, the arms were not identical. A realistic mesh was generated from a real sample (see fig.2). Then, a new sensitivity analysis was performed. Figure 11 shows the maps of displacement sensitivities. Surprisingly, the sensitivity is higher and better spread for all parameters than for idealized geometries. Interestingly, the sensitivity magnitude is similar for all parameters, especially for the k_2 parameter which was hardly identifiable in idealized geometries. The central part of the cross, in which the DIC is the easiest, has now non-zero sensitivities. Forces sensitivities (see fig. 12) reveal the same trend, with sensitivities to all the parameters.

Therefore, a non-symmetrical geometry is the more suitable for the identification of the Holzapfel constitutive behavior on a cross-shaped sample.

4 Discussion

As a connective soft tissue, skin is very complex to analyze: its properties are complex but also vary intra- and inter-individuals; they also change with time or due to external alterations. Despite many studies, the rela-

tionship between mechanical behavior and the skin microstructure remains poorly understood. To make further advances on this question, it is important to know which assay will provide the most useful information for the identification of the mechanical parameters. The aim of this work was to improve a biaxial assay so that it can be used to identify the five parameters of a hyperelastic non-linear constitutive equation including microstructural information in a single experiment. We chose the classical Holzapfel's law, since it is too complex to be identified accurately in a single experiment without field measurement. Still, our approach can easily be extended to any other constitutive law or other loading conditions. Nevertheless, in the case of biological tissues several tests have to be performing for statistically reasons.

Skin tissue has often been considered as linear, elastic, and incompressible. Thereby, a Young's modulus or a tangential modulus was often characterized by a Poisson's ratio close to 0.5 [16, 19, 20]. Other studies considered the skin as hyperelastic and isotropic, and characterized the parameters of Rivlin or Ogden models [31, 10]. In the present study, a hyperelastic model, incorporating information on the microstructure and with a natural anisotropy, was chosen so that it can be ultimately compared with experimental microstructural observations [5, 56, 60].

In this work, we performed $2D$ simulations under plane stress assumption. This assumes a uniformly thin thickness throughout the whole sample, and so we obtain only an average value of the thickness properties. As skin is a multilayer organ, with gradients of microstructure in the thickness [61], this may be too stringent for some fine-tuned models, or for the comparison

with experimental data which are generally obtained only near the surface. However, a full 3D model will be very complex to develop: it requests a depth-dependent constitutive law and fine information on the complex architecture of the tissue [1].

We also assumed lateral homogeneities of the mechanical properties (and of the fiber orientation). Previous experimental observations [5] have shown for the size of the middle part of our cross, the skin stretch is homogeneous. For large samples, it may be useful to allow lateral gradients of properties [62]. However, the quality of the identification will depend on the location, as the sensitivity is spatially heterogeneous (see for ex. fig.11). To determine heterogeneous properties, homogeneous tests (such as uniaxial traction on a perfect sample) will probably be more adequate.

We performed a careful sensitivity analysis that showed a high dependence on the geometry and loading path. Interestingly, non-symmetrical geometries and alternated loading are much more sensitive to all parameters of the tested model. The low sensitivity at the center of the symmetrical specimens was expected because there is a zero-displacement on the axes of symmetry that induced low strains. This is interesting as these conditions are easier to implement in real experiments than perfect symmetry. Cross-sensitivity between different parameters, and the lack of sensitivity of some parameters (such as k_2 here), need to be carefully analyzed when performing identification: they may lead to multivalued solutions and it may prevent the convergence of the identification as presented in [63]. It should be noted that, despite our confidence in the generality of our conclusions, we tested only one constitutive behavior and few configurations. The optimal loading

path and geometry may depend on the constitutive law to be identified, but, by extrapolation, we might consider that the complexity of loading and geometry is beneficial to the identification of anisotropic behavior. Therefore, this sensitivity analysis is essential to design experiments for an optimal parameter identification.

5 Conclusion

This study proposed an example of protocol improvement (*i.e.* loading and shape) through sensitivity analysis. The aim was to be able to identify the more precisely a hyperelastic constitutive behavior of soft tissues such as skin in a single assay so that we avoid inter-samples variability. This methodology allowed us to determine that an alternated loading and an non-symmetrical geometry are more efficient to determine the parameters of the Holzapfel's behavior, which are consistent with the increase of information in a given experiment. It also showed the heterogeneity of the sensitivity, illustrating in that case the importance of the field measurement of the stretch. The next step will consist of identifying the parameters on real measurements. Thus, the orientation index of fibers could be deduced and compared with microstructural observation (as obtained through Second Harmonic Generation microscopy [5]).

6 Acknowledgment

We thank Christelle Bonod-Bidaud for the skin sample preparation. This work was supported by grants from Agence Nationale de la Recherche ($ANR-13-BS09-0004$).

References

[1] Leyva-Mendivil, M. F., Page, A., Bressloff, N. W., and Limbert, G. A mechanistic insight into the mechanical role of the stratum corneum during stretching and compression of the skin. *Journal of the Mechanical Behavior of Biomedical Materials*, 2015, 49:197–219.

[2] Vitellaro-Zuccarello, L., Cappelletti, S., Rossi, V. D. P., and Sari-Gorla, M. Stereological analysis of collagen and elastic fibers in the normal human dermis: variability with age, sex, and body region. *The Anatomical Record*, 1994, 238(2):153–162.

[3] Frances, C., Branchet, M., Boisnic, S., Lesty, C., and Robert, L. Elastic fibers in normal human skin. variations with age: a morphometric analysis. *Archives of gerontology and geriatrics*, 1990, 10(1):57–67.

[4] Gogly, B., Godeau, G., Septier, D., Hornebeck, W., Pellat, B., and Jeandel, C. Measurement of the amounts of elastic fibers in the skin and temporal arteries of healthy aged individuals by automated image analysis. *Gerontology*, 1998, 44(6):318–323.

[5] Bancelin, S., Lynch, B., Bonod-Bidaud, C., Ducourthial, G., Psilodimitrakopoulos, S., Dokládal, P., Allain, J.-M., Schanne-Klein, M.-C., and Ruggiero, F. Ex vivo multiscale quantitation of skin biomechanics in wild-type and genetically-modified mice using multiphoton microscopy. *Scientific reports*, 2015, 5.

[6] Symoens, S., Syx, D., Malfait, F., Callewaert, B., De Backer, J., Vanakker, O., Coucke, P., and De Paepe, A. Comprehensive molec-

ular analysis demonstrates type v collagen mutations in over 90% of patients with classic eds and allows to refine diagnostic criteria. *Human mutation*, 2012, 33(10):1485–1493.

[7] Ricard-Blum, S. and Ruggiero, F. The collagen superfamily: from the extracellular matrix to the cell membrane. *Pathologie Biologie*, 2005, 53(7):430–442.

[8] Tregear, R. T. *Physical functions of skin*, volume 5. Academic Press, 1966.

[9] Frantz, C., Stewart, K. M., and Weaver, V. M. The extracellular matrix at a glance. *J Cell Sci*, 2010, 123(24):4195–4200.

[10] Veronda, D. and Westmann, R. Mechanical characterization of skinfinite deformations. *Journal of biomechanics*, 1970, 3(1):111–124.

[11] Holzapfel, G. A. Biomechanics of soft tissue. *The handbook of materials behavior models*, 2001, 3:1049–1063.

[12] Brown, I. A. A scanning electron microscope study of the effects of uniaxial tension on human skin. *British Journal of Dermatology*, 1973, 89(4):383–393.

[13] Park, A. C., Phillips, C. L., Pfeiffer, F. M., Roenneburg, D. A., Kernien, J. F., Adams, S. M., Davidson, J. M., Birk, D. E., and Greenspan, D. S. Homozygosity and heterozygosity for null col5a2 alleles produce embryonic lethality and a novel classic ehlers-danlos syndrome–related phenotype. *The American journal of pathology*, 2015.

[14] Cook, T., Alexander, H., and Cohen, M. Experimental method for determining the 2-dimensional mechanical properties of living human skin. *Medical and Biological Engineering and Computing*, 1977, 15(4):381–390.

[15] Hendriks, F., Brokken, D., Oomens, C., Bader, D., and Baaijens, F. The relative contributions of different skin layers to the mechanical behavior of human skin in vivo using suction experiments. *Medical engineering & physics*, 2006, 28(3):259–266.

[16] Hendriks, F., Brokken, D., Van Eemeren, J., Oomens, C., Baaijens, F., and Horsten, J. A numerical-experimental method to characterize the non-linear mechanical behaviour of human skin. *Skin research and technology*, 2003, 9(3):274–283.

[17] Diridollou, S., Patat, F., Gens, F., Vaillant, L., Black, D., Lagarde, J., Gall, Y., and Berson, M. In vivo model of the mechanical properties of the human skin under suction. *Skin Research and technology*, 2000, 6(4):214–221.

[18] Zheng, Y.-P. and Mak, A. F. An ultrasound indentation system for biomechanical properties assessment of soft tissues in-vivo. *Biomedical Engineering, IEEE Transactions on*, 1996, 43(9):912–918.

[19] Delalleau, A., Josse, G., Lagarde, J.-M., Zahouani, H., and Bergheau, J.-M. Characterization of the mechanical properties of skin by inverse analysis combined with the indentation test. *Journal of biomechanics*, 2006, 39(9):1603–1610.

[20] Delalleau, A., Josse, G., Lagarde, J.-M., Zahouani, H., and Bergheau, J.-M. A nonlinear elastic behavior to identify the mechanical parameters of human skin in vivo. *Skin Research and Technology*, 2008, 14(2):152–164.

[21] Tran, H., Charleux, F., Rachik, M., Ehrlacher, A., and Ho Ba Tho, M. In vivo characterization of the mechanical properties of human skin derived from mri and indentation techniques. *Computer methods in biomechanics and biomedical engineering*, 2007, 10(6):401–407.

[22] Jacquet, E., Josse, G., Khatyr, F., and Garcin, C. A new experimental method for measuring skin's natural tension. *Skin Research and technology*, 2008, 14(1):1–7.

[23] Finlay, B. The torsional characteristics of human skin in vivo. *Biomedical engineering*, 1971, 6(12):567–573.

[24] Manduca, A., Oliphant, T. E., Dresner, M., Mahowald, J., Kruse, S., Amromin, E., Felmlee, J. P., Greenleaf, J. F., and Ehman, R. L. Magnetic resonance elastography: non-invasive mapping of tissue elasticity. *Medical image analysis*, 2001, 5(4):237–254.

[25] Bercoff, J., Tanter, M., and Fink, M. Supersonic shear imaging: a new technique for soft tissue elasticity mapping. *Ultrasonics, Ferroelectrics, and Frequency Control, IEEE Transactions on*, 2004, 51(4):396–409.

[26] Sandrin, L., Tanter, M., Gennisson, J.-L., Catheline, S., and Fink, M. Shear elasticity probe for soft tissues with 1-d transient elastography.

Ultrasonics, Ferroelectrics, and Frequency Control, IEEE Transactions on, 2002, 49(4):436–446.

[27] Moerman, K. M., Holt, C. A., Evans, S. L., and Simms, C. K. Digital image correlation and finite element modelling as a method to determine mechanical properties of human soft tissue in vivo. *Journal of biomechanics*, 2009, 42(8):1150–1153.

[28] Evans, S. L. and Holt, C. A. Measuring the mechanical properties of human skin in vivo using digital image correlation and finite element modelling. *The Journal of Strain Analysis for Engineering Design*, 2009, 44(5):337–345.

[29] Cox, M. A., Driessen, N. J., Boerboom, R. A., Bouten, C. V., and Baaijens, F. P. Mechanical characterization of anisotropic planar biological soft tissues using finite indentation: experimental feasibility. *Journal of biomechanics*, 2008, 41(2):422–429.

[30] Genovese, K., Montes, A., Martínez, A., and Evans, S. L. Full-surface deformation measurement of anisotropic tissues under indentation. *Medical engineering & physics*, 2015, 37(5):484–493.

[31] Ogden, R. W. *Non-linear elastic deformations*. Courier Corporation, 1997.

[32] Fung, Y. *Biomechanics: Mechanical Properties of Living Tissues*. Springer-Verlag, New York, 1993.

[33] Holzapfel, G. A., Gasser, T. C., and Ogden, R. W. A new constitutive framework for arterial wall mechanics and a comparative study of ma-

terial models. *Journal of elasticity and the physical science of solids*, 2000, 61(1-3):1–48.

[34] Jansen, L. and Rottier, P. Elasticity of human skin related to age. *Dermatology*, 1957, 115(2):106–111.

[35] Daly, C. H. Biomechanical properties of dermis. *Journal of Investigative Dermatology*, 1982, 79:17–20.

[36] Iatridis, J. C., Wu, J., Yandow, J. A., and Langevin, H. M. Subcutaneous tissue mechanical behavior is linear and viscoelastic under uniaxial tension. *Connective Tissue Research*, 2003, 44(5):208–217.

[37] Silver, F. H., Freeman, J. W., and DeVore, D. Viscoelastic properties of human skin and processed dermis. *Skin Research and Technology*, 2001, 7(1):18–23.

[38] Pan, L., Zan, L., and Foster, F. S. Ultrasonic and viscoelastic properties of skin under transverse mechanical stress in vitro. *Ultrasound in medicine & biology*, 1998, 24(7):995–1007.

[39] Ridge, M. and Wright, V. A bio-engineering study of the mechanical properties of human skin in relation to its structure. *British Journal of Dermatology*, 1965, 77(12):639–649.

[40] Kang, G. and Wu, X. Ratchetting of porcine skin under uniaxial cyclic loading. *Journal of the mechanical behavior of biomedical materials*, 2011, 4(3):498–506.

[41] Waldman, S. D. and Lee, J. M. Effect of sample geometry on the apparent biaxial mechanical behaviour of planar connective tissues. *Biomaterials*, 2005, 26(35):7504–7513.

[42] Waldman, S. D. and Lee, J. M. Boundary conditions during biaxial testing of planar connective tissues. part 1: dynamic behavior. *Journal of materials science: Materials in medicine*, 2002, 13(10):933–938.

[43] Lanir, Y. and Fung, Y. Two-dimensional mechanical properties of rabbit skini. experimental system. *Journal of Biomechanics*, 1974, 7(1):29–34.

[44] Lanir, Y. and Fung, Y. Two-dimensional mechanical properties of rabbit skinii. experimental results. *Journal of biomechanics*, 1974, 7(2):171–182.

[45] Lanir, Y. A structural theory for the homogeneous biaxial stress-strain relationships in flat collagenous tissues. *Journal of biomechanics*, 1979, 12(6):423–436.

[46] Reihsner, R., Balogh, B., and Menzel, E. Two-dimensional elastic properties of human skin in terms of an incremental model at the in vivo configuration. *Medical engineering & physics*, 1995, 17(4):304–313.

[47] Schneider, D. C., Davidson, T. M., and Nahum, A. M. In vitro biaxial stress-strain response of human skin. *Archives of Otolaryngology*, 1984, 110(5):329–333.

[48] Jor, J. W., Nash, M. P., Nielsen, P. M., and Hunter, P. J. Estimating material parameters of a structurally based constitutive relation for

skin mechanics. *Biomechanics and modeling in mechanobiology*, 2011, 10(5):767–778.

[49] Eilaghi, A., Flanagan, J. G., Brodland, G. W., and Ethier, C. R. Strain uniformity in biaxial specimens is highly sensitive to attachment details. *Journal of biomechanical engineering*, 2009, 131(9):091003.

[50] Sacks, M. S. Biaxial mechanical evaluation of planar biological materials. *Journal of elasticity and the physical science of solids*, 2000, 61(1-3):199–246.

[51] Jacobs, N. T., Cortes, D. H., Vresilovic, E. J., and Elliott, D. M. Biaxial tension of fibrous tissue: using finite element methods to address experimental challenges arising from boundary conditions and anisotropy. *Journal of biomechanical engineering*, 2013, 135(2):021004.

[52] Nolan, D. and McGarry, J. On the correct interpretation of measured force and calculation of material stress in biaxial tests. *Journal of the mechanical behavior of biomedical materials*, 2016, 53:187–199.

[53] Schmaltz, S. and Willner, K. Comparison of different biaxial tests for the inverse identification of sheet steel material parameters. *Strain*, 2014, 50(5):389–403.

[54] Bertin, M., Hild, F., and Roux, S. Optimization of a cruciform specimen geometry for the identification of constitutive parameters based upon full-field measurements. *Strain*, 2016.

[55] Palanca, M., Tozzi, G., and Cristofolini, L. The use of digital image correlation in the biomechanical area: a review. *International biomechanics*, 2016, 3(1):1–21.

[56] Lynch, B., Bancelin, S., Bonod-Bidaud, C., Gueusquin, J.-B., Ruggiero, F., Schanne-Klein, M.-C., and Allain, J.-M. A novel microstructural interpretation for the biomechanics of mouse skin derived from multiscale characterization. *Acta Biomaterialia*, 2016.

[57] Bornert, M., Hild, F., Orteu, J.-J., and Roux, S. Digital image correlation. *Full-Field Measurements and Identification in Solid Mechanics*, 2012, pages 157–190.

[58] Gasser, T. C., Ogden, R. W., and Holzapfel, G. A. Hyperelastic modelling of arterial layers with distributed collagen fibre orientations. *Journal of the royal society interface*, 2006, 3(6):15–35.

[59] Systèmes, D. Abaqus 6.14 online documentation. 2014, 2015.

[60] Jayyosi, C., Affagard, J.-S., Ducourthial, G., Bonod-Bidaud, C., Lynch, B., Bancelin, S., Ruggiero, F., Schanne-Klein, M.-C., Allain, J.-M., Bruyère-Garnier, K., et al. Affine kinematics in planar fibrous connective tissues: an experimental investigation. *Biomechanics and Modeling in Mechanobiology*, 2017, pages 1–15.

[61] Silver, F., Kato, Y., Ohno, M., and Wasserman, A. Analysis of mammalian connective tissue: relationship between hierarchical structures and mechanical properties. *Journal of long-term effects of medical implants*, 1991, 2(2-3):165–198.

[62] Avril, S. and Evans, S., editors. *Material Parameter Identification and Inverse Problems in Soft Tissue Biomechanics*, volume 573 of *CISM International Centre for Mechanical Sciences*. Springer International Publishing, 2017.

[63] Molimard, J., Le Riche, R., Vautrin, A., and Lee, J.-R. Identification of the four orthotropic plate stiffnesses using a single open-hole tensile test. *Experimental mechanics*, 2005, 45(5):404–411.

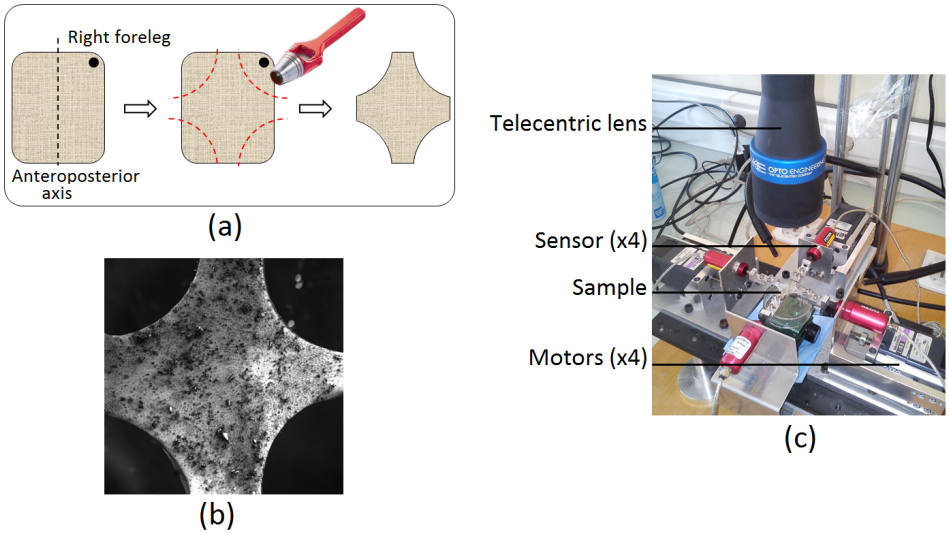

Figure 1: *a) Illustration of the sample cutting procedure. b) Sample covered with graphite powder for the measurement of the displacement field. c) Custom-made device.*

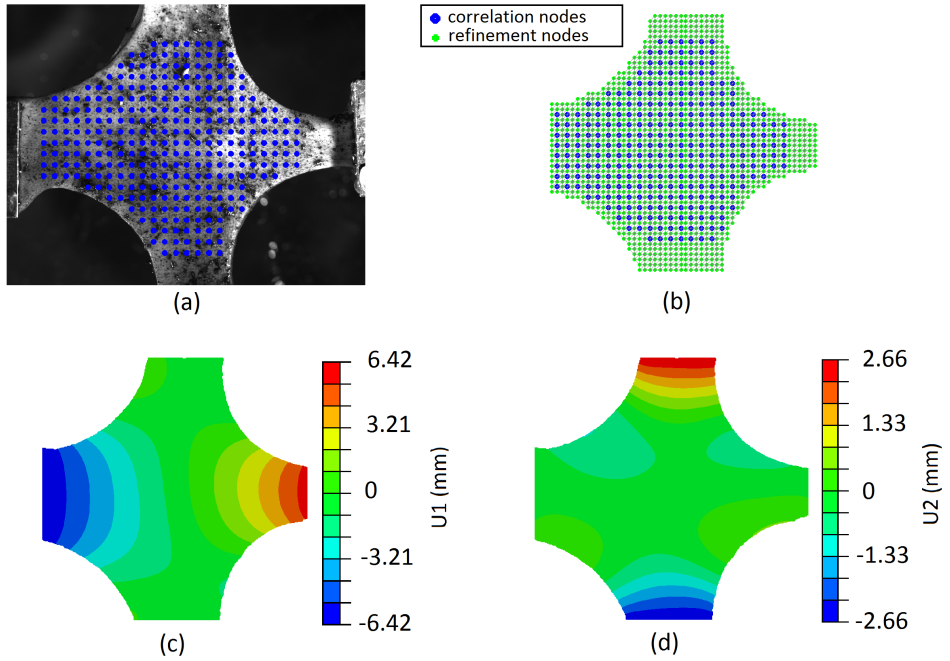

Figure 2: *Finite Element reproduction of an experimental geometry. (a) Image of the skin just before stretching (reference configuration). The dots are the positions of the correlation points used in the DIC. (b) Realistic FE mesh. The geometry of the mesh was extracted from the reference image, and the mesh was designed so that a subset of points is associated with the correlation points. The refinement is here 2 (the element side length is* $86px$*). (c-d) FE displacement fields* U_1 *and* U_2 *respectively in the horizontal and vertical directions for an imposed stretch of* 1.1 *in direction* 1 *and of* 1.2 *in direction* 2 *with* $\alpha = 10°$, $C_{10} = 40kPa$, $k_1 = 0.8kPa$, $k_2 = 0.5$ *and* $\kappa = 0.28$.

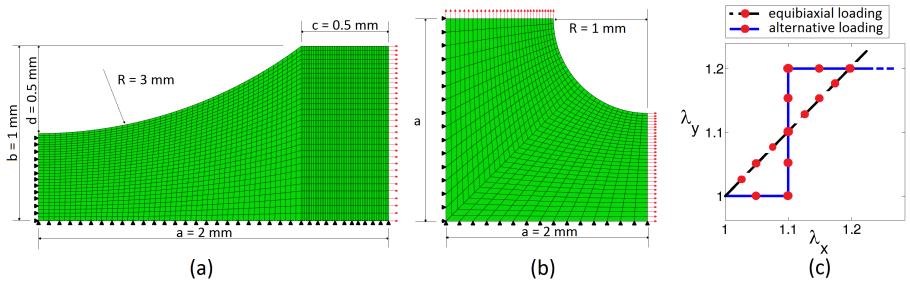

Figure 3: *Idealized geometry for sensitivity analysis. a-b) FE meshes of the quarter plate respectively for the uniaxial and biaxial experiments. c) Tested loading paths: equibiaxial (dotted) and alternative (plain)*

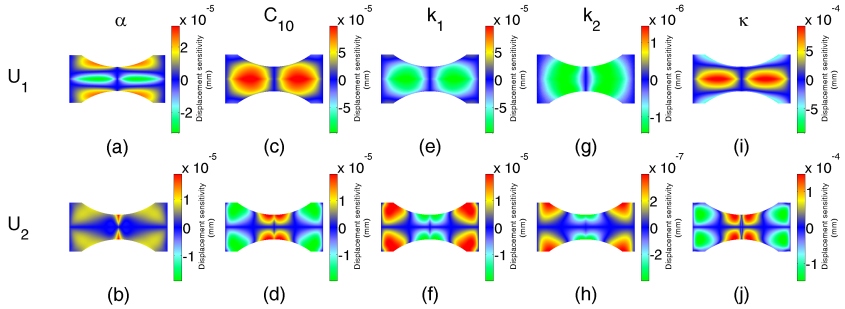

Figure 4: *Cartographies of the displacement sensitivity for the uniaxial loading experiment: a) angle for U_1, b) angle for U_2, c) C_{10} for U_1, d) C_{10} for U_2, e) k_1 for U_1, f) k_1 for U_2 , g) k_2 for U_1, h) k_2 for U_2, i) κ for U_1, j) κ for U_2.*

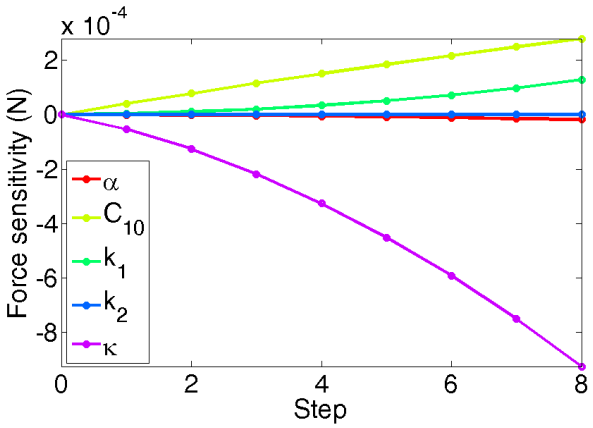

Figure 5: *Evolution of the force sensitivity for the uniaxial loading experiment*

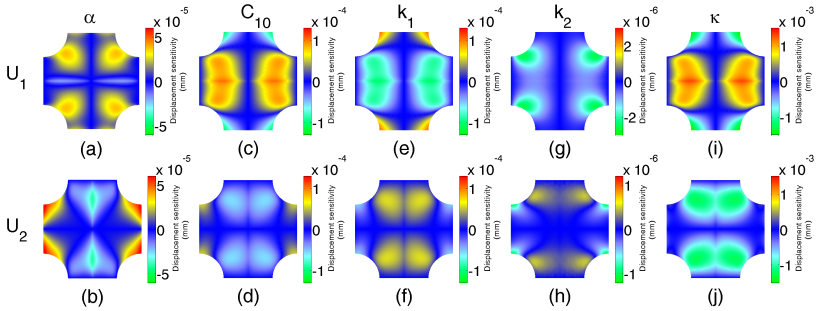

Figure 6: *Cartographies of the displacement sensitivity for the equibiaxial loading experiment: a) angle for U_1, b) angle for U_2, c) C_{10} for U_1, d) C_{10} for U_2, e) k_1 for U_1, f) k_1 for U_2 , g) k_2 for U_1, h) k_2 for U_2, i) κ for U_1, j) κ for U_2.*

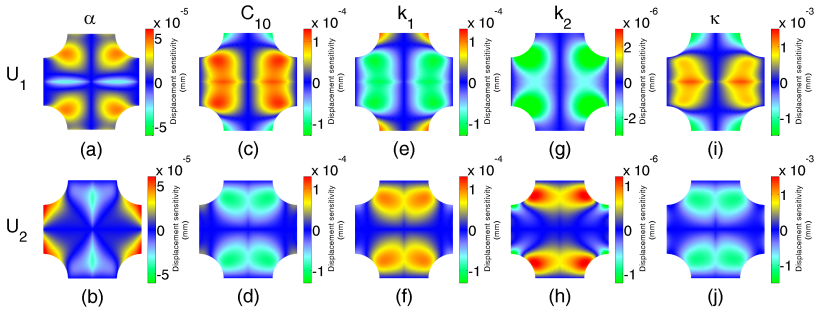

Figure 7: *Cartographies of the displacement sensitivity for the alternated loading experiment: a) angle for U_1, b) angle for U_2, c) C_{10} for U_1, d) C_{10} for U_2, e) k_1 for U_1, f) k_1 for U_2 , g) k_2 for U_1, h) k_2 for U_2, i) κ for U_1, j) κ for U_2.*

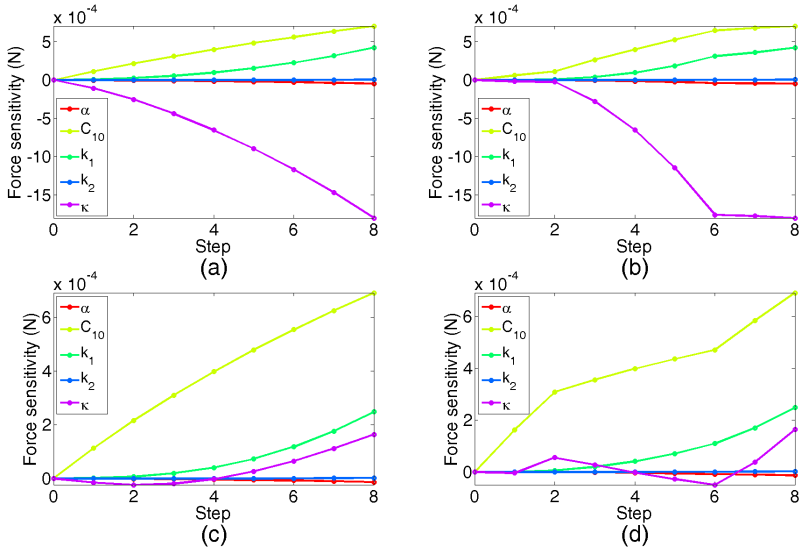

Figure 8: *Evolution of the force sensitivity for the biaxial experiment. a) F_1 and b) F_2 for the equibiaxial experiment. c) F_1 and d) F_2 for the alternated experiment.*

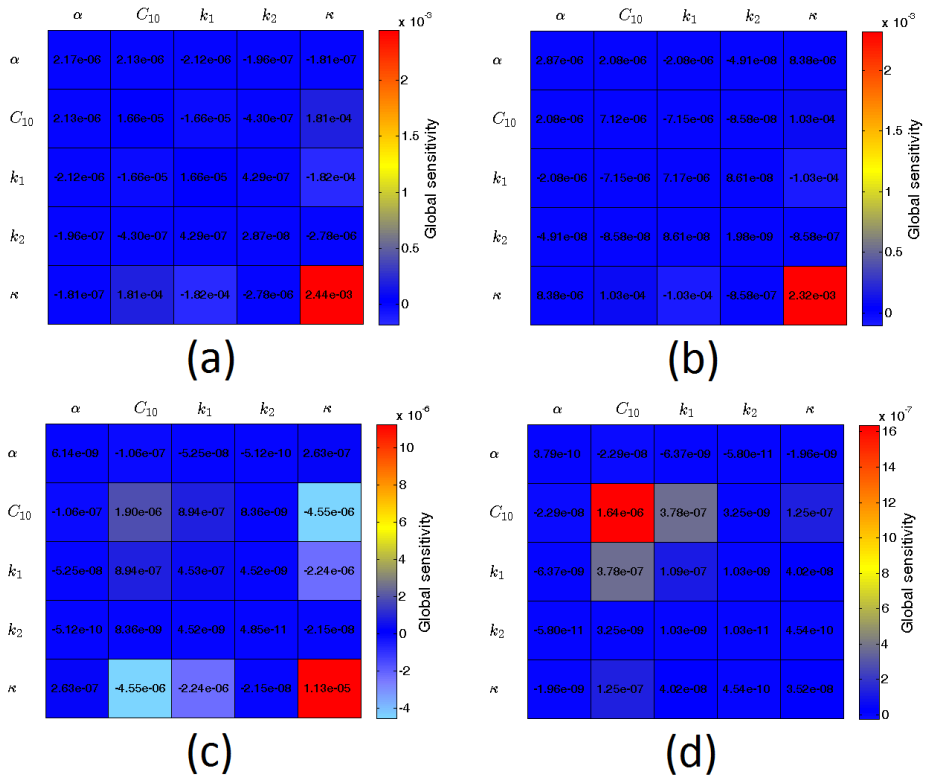

Figure 9: *Sensitivity matrices of the alternated experiment: a) U_1 b) U_2 c) F_1 d) F_2.*

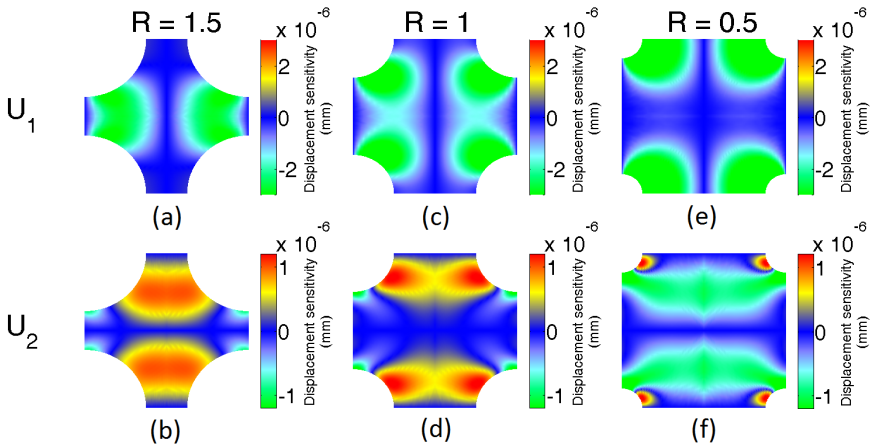

Figure 10: *Cartographies of the displacement sensitivity for the alternated loading experiment applied to several radius: a)* $R = 1.5mm$*, b)* $R = 1mm$*, c)* $R = 0.5mm$

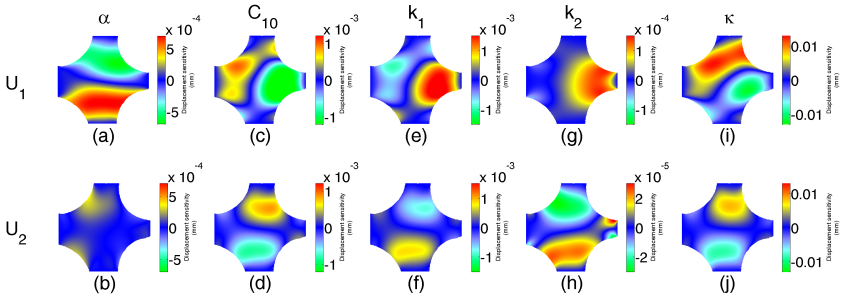

Figure 11: *Cartographies of the displacement sensitivity for the alternated loading experiment applied to a real geometry: a) angle for* U_1*, b) angle for* U_2*, c)* C_{10} *for* U_1*, d)* C_{10} *for* U_2*, e)* k_1 *for* U_1*, f)* k_1 *for* U_2 *, g)* k_2 *for* U_1*, h)* k_2 *for* U_2*, i)* κ *for* U_1*, j)* κ *for* U_2*.*

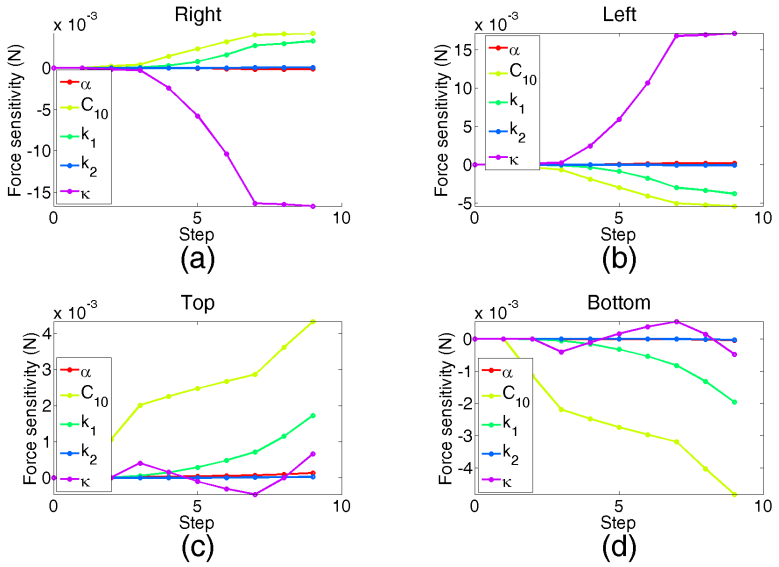

Figure 12: *Evolution of the a) F_1 and b) F_2 sensitivity for the alternated experiment applied to a real geometry.*